

# Optical remote sensing of submerged aquatic vegetation: opportunities for shallow clear water streams

Fleur Visser\*, Caroline Wallis, Anne Sinnott  
Institute of Science and the Environment, University of Worcester,  
Henwick Grove, Worcester, WR2 6AJ, United Kingdom

\*Corresponding author. Tel.: +44 1905 855236. E-mail address: [f.visser@worc.ac.uk](mailto:f.visser@worc.ac.uk).

Running title: Remote sensing of submerged vegetation in clear streams

Keywords: Submerged aquatic vegetation, shallow rivers, optical remote sensing, object-based image analysis, very high resolution image data

## Abstract

Remote sensing has rarely been used as a tool to map and monitor submerged aquatic vegetation (SAV) in rivers, due to a combination of insufficient spatial resolution of available image data and strong attenuation of light in water through absorption and scattering. The latter process reduces the possibility to use spectral reflectance information to accurately classify submerged species. However, increasing availability of Very High Resolution (VHR) image data may enable the use of shape and texture features to help discriminate between species by taking an Object Based Image Analysis (OBIA) approach, and overcome some of the present limitations.

This study aimed to investigate the possibility of using optical remote sensing for the detection and mapping of SAV. It firstly looked at the possibilities to discriminate submerged macrophyte species based on spectral information only. Reflectance spectra of three macrophyte species were measured *in-situ* across a range of submergence depths. The results showed that water depth will be a limiting factor for the classification of species from remote sensing images. Only Spiked Water Milfoil (*Myriophyllum spicatum*) was indicated as spectrally distinct through ANOVA analysis, but subsequent Jeffries-Matusita distance analysis did not confirm this. In particular Water Crowfoot (*Ranunculus fluitans*) and Pondweed (*Potamogeton pectinatus*) could not be discriminated at 95% significance level. Spectral separability of these two species was also not possible without the effect of an overlying water column.

Secondly, the possibility to improve species discrimination, using spatial and textural information was investigated for the same SAV species. VHR image data was acquired with a Near Infrared (NIR) sensitive DSLR camera from four different heights including a telescopic pole and a Helikite UAS. The results show that shape and texture information can improve the detection of the spectrally similar Pondweed and Water Crowfoot from VHR image data. The best performing feature 'length/width ratio of sub-objects' was obtained through expert knowledge. All of the shape and texture based features performed better at species differentiation than the spectrally based features.

In conclusion this study has shown that there is considerable potential for the combination of VHR data and OBIA to map SAV in shallow stream environments, which can benefit species monitoring and management.

## Introduction

Collecting data on submerged aquatic vegetation (SAV) from fluvial environments, which sufficiently represent spatial variation along a river reach, is difficult to achieve and often requires destructive and labour-intensive fieldwork (e.g. Flynn et al., 2002). Methods to obtain information remotely could therefore be of great benefit to the field of river science, including ecohydraulics. However, a combination of insufficient spatial resolution of image data and strong attenuation of light in water through absorption and scattering has long been a barrier for the application of remote

51 sensing technology to study fluvial environments (Gilvear et al., 2007; Marcus and Fonstad, 2008).  
52 This paper describes a project that applies a set of novel remote sensing techniques to map SAV,  
53 which could help overcome some of these limitations.

54  
55 Remote sensing has so far rarely been used as a tool to map and monitor submerged aquatic  
56 vegetation in rivers (Marcus and Fonstad, 2008). A recent study by Lee et al. (2011) is one of the first  
57 to look at the feasibility of using airborne hyperspectral image data to map SAV communities in  
58 rivers. They studied the separability of four vegetation types in small rivers in western Nevada, US,  
59 which included submerged brown and green filamentous algae communities. In the UK Hill et al.  
60 (2009) were some of the first to attempt estimating submerged vegetation biomass (Water Crowfoot)  
61 from image data taken with an airborne hyperspectral sensor. They did this for the River Frome chalk  
62 stream. Although a reasonable estimate could be made, the success of this analysis was severely  
63 limited by the quality and spatial resolution of the data (>1m) (Visser and Hill, 2011). Clearly further  
64 work is required in this field.

65 While for terrestrial applications light in the near infrared wavelengths (NIR) is particularly  
66 useful for the detection of variation in vegetation cover, the absorption characteristics of water limit  
67 its use for SAV. As a result of both absorption by water and scattering by particles, light is attenuated  
68 with distance travelled through the water column. In the optical range of the electromagnetic spectrum  
69 NIR is more strongly absorbed by water than the visible wavelengths (VIS). NIR can therefore only  
70 be used in image data of very shallow aquatic environments (< ~1m) to provide any information about  
71 bottom features. It also means that in sufficiently shallow aquatic environments variation in recorded  
72 NIR reflectance does not only reflect variation in vegetation types or condition, but also variation in  
73 the depth of the plant below the water surface. When applying optical imagery to map SAV, this  
74 results in an unfortunate situation, which is described by Hedley et al. (2012) as 'environmentally  
75 limited remote sensing'. Variation in depth, variation in the reflectance signatures of the bottom  
76 substrate or cover types and potentially other factors such as water clarity, together contribute to  
77 overall variation in the signal recorded by an image sensor and can lead to an overlap between two or  
78 more mapped vegetation classes.

79 Hedley et al. (2012) focussed on such environmental limitations in Australian marine  
80 environments. Generally more work has been done on remote sensing of SAV in marine environments  
81 and various attempts have been made to resolve complications of submerged situations. O'Neill et al.  
82 (2011) for example used information about submergence depth to adjust above water reflectance  
83 spectra for attenuation influence, using the empirical water attenuation correction by Maritorena et al.  
84 (1994). O'Neill et al. (2011) had access to a depth dataset and managed to produce a 97% overall  
85 classification accuracy for Eelgrass detection. Depth data of sufficient quality is however not usually  
86 available and certainly not of the detail required for fluvial environments. Lidar and radar data which  
87 work for terrestrial situations again do not (yet) perform well enough in submerged fluvial conditions  
88 (e.g. Wang and Philpot, 2007). Important progress is being made with the application of inversion of  
89 modeling of bio-optical models (e.g. Dekker et al. (2011) for marine environment and Giardino et al.  
90 (2012) for lacustrine settings). Legleiter and Roberts (2009) explored the potential of inverse  
91 modelling with regards to accuracy and precision methods for fluvial environments, using data  
92 simulated with a forward image model (FIM). They found they methods would be suitable for depth  
93 retrieval. However, data and analysis techniques are still insufficient to successfully apply them in  
94 fluvial environments.

95  
96 The foregoing overview identified how a combination of insufficient spatial and spectral  
97 resolution of available image data, has so far ruled out their use for studies of smaller rivers (width <  
98 10m). However ongoing improvements of image data collection and image analysis techniques are  
99 finally changing this situation. Unmanned Aerial Systems (UAS), which are small, low-altitude  
100 remote sensing platforms such as small fixed winged planes or mini-helicopters, are rapidly  
101 developing into relatively cheap and logistically flexible means to obtain Very High Resolution  
102 (VHR) multi-spectral image data. When classifying a remote sensing image to obtain maps of  
103 submerged environments (e.g. SAV or river bed morphology) VHR data has the advantage that it can

104 generate detailed information on aspects of shape, structure and texture of the target surface. Using  
105 so-called ‘Object Based Image Analysis’ (OBIA) techniques this information can be incorporated in  
106 the image analysis process to improve an image classification originally based on spectral information  
107 only (e.g. Van der Werff and Van der Meer, 2008 and Laliberté and Rango, 2009). While  
108 conventional image analysis techniques derive information about the target spectral reflectance on a  
109 pixel by pixel basis, OBIA first segments the image data into spectrally homogenous objects. For each  
110 object it then quantifies feature values such as shape (e.g. roundness or length/width ratio), internal  
111 texture and characteristics of adjacent objects (e.g. contrast to neighbouring object). When such  
112 additional object feature values are included in the analysis algorithm they can considerably improve  
113 image classification (e.g. Blaschke et al., 2011).

114

115 The study aimed to establish application of remote sensing methods for fluvial environments  
116 and better appreciate the inherent limitations as identified by Hedley et al. (2012). This was done by  
117 meeting the following two objectives:

- 118 – Determine the possibility to discriminate between three submerged macrophyte species based  
119 on spectral information only.
- 120 – Determine whether discrimination of the same species could be improved using spatial and  
121 textural information obtained from VHR image data.

122

## 123 **Methods**

### 124 *Introduction*

125 Statistically discriminating between surface (cover) types based on spectral information, lies  
126 at the basis of classification of remote sensing image data. For this purpose spectral information about  
127 the cover types is usually obtained from a training sample of pixels in the image. If separability  
128 between the samples is higher, cover types can be mapped from the image more reliably. In order to  
129 check whether classification is possible in the first place and to find the optimal wavelength bands (or  
130 band combinations) to do this, a considerable number of studies have also investigated separability of  
131 sets of individual spectra from cover types measured *in-situ* (e.g. Vahtmäe et al., 2006; Karpouzli et  
132 al., 2004; O’Neill et al., 2011; Lee et al., 2011). In this study a GER1500 hand-held field  
133 spectroradiometer was used to collect reflectance spectra *in-situ* from the three submerged  
134 macrophyte species across a range of submergence depths.

135 Remote sensing image classification processing time increases with the number of spectral  
136 bands associated with a pixel, so techniques to assess separability between classes usually involve a  
137 reduction in data dimensionality. A range of techniques have been applied to determine separability of  
138 cover types, based on samples of in situ reflectance spectra (e.g. Lee et al., 2011; O’Neill et al., 2011;  
139 Adam and Mutanga, 2009). This suggests that there is no consensus on what method is most suitable.  
140 This observation is confirmed by Adam and Mutanga (2009) and Yang et al. (2005). Here we use the  
141 methodology of Adam and Mutanga (2009), who took a hierarchical approach to reduce the  
142 dimensionality of their data before determining species separability. One-way ANOVA was used with  
143 a post-hoc Scheffé test to determine for each wavelength band which macrophyte pairs were  
144 significantly different. This was followed by Classification And Regression Trees (CART) analysis  
145 (Breiman et al., 1984) to select the most suitable bands for species discrimination.

146 A trained observer will be able to distinguish between Pondweed and Water Crowfoot by  
147 looking at their photographs despite their similar green colour. Their interpretation or ‘classification’  
148 of the image will therefore involve more than the clustering of spectral values, as done in the first part  
149 of this study. OBIA attempts to simulate these additional human cognitive processes in order to  
150 improve image classification based on clustering of spectral values only. Recent studies by Phinn et  
151 al. (2012) and Urbanski et al. (2009) have shown the benefit of this kind of approach for marine  
152 environments. The second part of this study therefore investigates the possibility to improve  
153 discrimination of the same three SAV species from image data, using spatial and textural information  
154 in addition to the spectral information. VHR image data for this part of the study is acquired with a

155 Near Infrared (NIR) sensitive DSLR camera. Images are taken from four different heights, in order to  
156 understand how the OBIA approach is affected by the scale of the image data. The platforms used to  
157 achieve this include a telescopic pole and a Helikite UAS.

### 158 *Study sites*

159 The field sites for this study were located along two UK chalk streams: the River Wylye in  
160 Wiltshire and the River Frome in Dorset. These calcareous groundwater-fed streams were selected  
161 because of their exceptional water clarity and abundance of a range of macrophyte species. Most data  
162 were obtained from the River Wylye at Steeple Langford where it flows through the Langford Trust  
163 nature reserve in Wiltshire. Additional data was collected from a tributary of the River Frome near  
164 Wool in Dorset. The sites were physically very similar, with a stream width of around 5m and a  
165 maximum water depth at time of sampling of around 50cm. Although this study involves one  
166 particular type of stream only, the techniques and issues discussed are likely to apply to a much wider  
167 range of clear water streams with SAV and to some extent also shallow lake environments.

168 The study focuses on three macrophyte species commonly found in the chalk streams: Water  
169 Crowfoot (*Ranunculus fluitans*), Pondweed (*Potamogeton pectinatus*) and Spiked Water Milfoil  
170 (*Myriophyllum spicatum*). Water Crowfoot is a keystone species of high conservation value for chalk  
171 stream environments. The habitats they form are protected under the European Union Habitats and  
172 Species Directive (92/43/EEC) (O'Hare et al., 2010). Management of the species is therefore a trade-  
173 off between conservation and growth control for fisheries and flood management. Remote sensing  
174 could make an important contribution to improved management practices. The other two species were  
175 chosen because of their relative abundance at the field sites and because pondweed is spectrally very  
176 similar to Water Crowfoot, but structurally rather different, while the opposite is the case for Water  
177 Milfoil.

### 178 *Spectral measurements of submerged aquatic vegetation*

179 To collect reflectance spectra from three submerged macrophyte species, measurements took  
180 place with a GER1500 hand-held field spectroradiometer over several days in late August and early  
181 September of 2009 and 2010 at both field sites. Due to limited access to the river and limited  
182 availability of specific vegetation species at different depths purposive sampling was applied to obtain  
183 submerged vegetation spectra at a range of submergence depths. To obtain spectra of vegetation  
184 without water column influences multiple layers of vegetation were piled on black painted canvas.  
185 The GER1500 was held at nadir 50cm above the water surface or canvas. The instrument has a 3°  
186 field of view so the area measured on the target has a 2.6 – 4.0cm diameter (depending on  
187 submergence depth), which is assumed sufficient to obtain representative spectral information from  
188 the dense vegetation stands. Sampling was carried out on cloud-free days within 2 hours of solar  
189 noon. Spectral averaging of 10–30 spectra per sample was performed to ensure optimal signal-to-  
190 noise ratio. A white reference Spectralon calibration panel of 99% reflectance was used every 5 to 10  
191 samples to offset any change in the atmospheric condition and irradiance of the sun. Reflectance was  
192 calculated by dividing macrophyte radiance by radiance from the Spectralon surface.

### 193 *ANOVA and CART Analysis species discrimination*

194 To analysis species discrimination we used the methodology of Adam and Mutanga (2009).  
195 They took a hierarchical approach to reduce the dimensionality of their data before determining  
196 species separability. This first involves a statistical test of differences in mean reflectance values for  
197 all combinations of two macrophyte species at each measured wavelength (350 to 1050 nm):

198  
199  $H_0 : \mu_1(i) = \mu_2(i) = \mu_3(i)$   
200  $H_1 : \text{at least one } \mu(i) \text{ is different}$

201  
202 where  $\mu_1$ -3 represent the mean reflectance of the 3 macrophyte species and  $i$  denotes the  
203 spectral wavelength band. One-way ANOVA was used with a post-hoc Scheffé test to determine for

204 each wavelength band which macrophyte pairs were significantly different. ANOVA was tested for  
 205 99% and 95% confidence levels ( $p < 0.01$  and  $p < 0.05$ ). For each wavelength band the number of  
 206 significantly different macrophyte species combinations were counted (in this case max. 3) to  
 207 determine the wavelength bands most suitable for spectral discrimination. The one-way ANOVA  
 208 coupled with a post-hoc pair-wise comparison resulted in a frequency plot of statistically significant  
 209 mean reflectance values for each wavelength.

210 Although significant difference for the ANOVA test indicates at which wavelengths species  
 211 are most likely to be spectrally different, it does not guarantee separability of the macrophyte species  
 212 based on individual wavelength bands from this region. A measure for correct classification of the  
 213 vegetation types from image data using a single or combination of multiple bands can be determined  
 214 by calculating Jeffries–Matusita (J–M) distance values. However, it is very time consuming to  
 215 calculate the distance measure for all possible combinations of the bands identified by ANOVA.  
 216 Adam and Mutanga (2009) therefore performed a further step to select the most suitable bands for  
 217 species discrimination, using the Classification And Regression Trees (CART) approach (Breiman et  
 218 al., 1984). CART is a form of binary recursive partitioning that permits accurate prediction or  
 219 classification of cases, using both continuous and categorical variables. Training data is used to  
 220 identify ‘splitting’ variables based on an exhaustive search of possible variable combinations.  
 221 Repeated partitioning of the data with additional variables occurs until criteria for predictive accuracy  
 222 are met. This automatically results in the optimal number of bands for separation of all  
 223 classes/species.

224 For this study we did CART analysis using the bands from 99% confidence level regions as  
 225 input and compared the results with CART analysis using the full set of bands to confirm the benefit  
 226 of initial band selection through ANOVA. Each tree/model was validated with a test sample of at least  
 227 25%. Because we were particularly interested in the possibility to separate the spectrally very similar  
 228 Pondweed and Water Crowfoot, additional CART band selection was performed including these two  
 229 species only and the results will also be presented.

230 Finally Jeffries–Matusita (J–M) distance values were calculated for the wavelength band  
 231 combinations selected by the CART method. To determine to what extent improvement of species  
 232 separation was achieved at the different stages of the analysis process, we also calculated J-M values  
 233 for 5 sets of 5 band combinations ranging from 2-6 bands which were randomly selected from the  
 234 ANOVA 99% confidence level regions only, as well as J-M values for 5 sets of 5 band combinations  
 235 ranging from 2-6 bands selected at random from the 741 bands included in the analysis. The square of  
 236 the J–M distance values ranges between 0 and 2, with larger J–M distance values indicating greater  
 237 separability between group pairs. Values greater than 1.9 indicate that the sample pairs have good  
 238 separability (ENVI, 2004).

239  
 240 
$$J - M_{ij} = \sqrt{2(1 - e^{-\alpha})} \quad 1$$

241  
 242 With  
 243

244 
$$\alpha = \frac{1}{8}(\mu_i - \mu_j)^T \left( \frac{C_i + C_j}{2} \right)^{-1} (\mu_i - \mu_j) + 2 \ln \left( \frac{\binom{1}{2} |C_i + C_j|}{\sqrt{|C_i| |C_j|}} \right) \quad 2$$

245  
 246 Where i and j are the two species compared;  $C_i$ = covariance matrix of the spectral response of i;  $\mu_i$  =  
 247 the mean vector of signature of i; T = transposition function;  $|C_i|$  = the determinant of  $C_i$ .

248

249 *Collection of VHR image data*

250 Next we tested the usefulness of a range of image object features such as shape and texture to  
251 distinguish between macrophyte species in shallow rivers. We focused only on the two spectrally  
252 most similar macrophyte species Water Crowfoot and Pondweed. The analysis was applied to a set of  
253 four multi-spectral images, which included stands of both species. All images were taken with the  
254 same camera from four 'platforms' at different heights above the water surface in order to evaluate the  
255 applicability of shape and texture features for species detection across a range of scales. The platforms  
256 included a tripod located in the river near a bridge at 1.5m elevation (location: 'from tripod'), from a  
257 bridge at 3m (location: 'from bridge'), from a telescopic pole at 5.4m (location: 'from pole') and  
258 from a Helikite UAS (a combined helium balloon and kite) at about 5m elevation (location: 'from  
259 helikite').

260 Despite strong absorption of NIR light in water, spectral signatures of submerged  
261 macrophytes measured with the GER1500 field spectroradiometer, indicated that light in these  
262 wavelengths may be useful in image classification (Visser and Wallis, 2010). Initial inspection of  
263 NIR images also showed that plant structure and shape features appeared more strongly pronounced  
264 in this wavelength region. Because sufficiently light-weight multispectral sensors suitable for small  
265 UAS-s are not available yet, multi-spectral images have been created with a Fujifilm IS-Pro NIR  
266 sensitive DSLR camera on a layer by layer basis, taking repeated photos of the same location and  
267 stacking these subsequently using GIS software. A NIR blocking filter was used on the camera to  
268 obtain Red, Green and Blue image bands, A VIS blocking filter was used to obtain a band covering  
269 most of the NIR spectrum (R72) and a bandpass filter was used to obtain a narrow NIR wavelength  
270 band round 710nm (NIR (BP1)). Figure 1 shows the filter transmission spectra and their specifications  
271 are as follows:

- 272 – R, G, B: MaxMax X-Nite CC1 NIR blocking filter (centre: 483nm; 50% transmission:  
273 325nm, 645nm)
- 274 – NIR(R72): Hoya R72 VIS blocking filter (<720nm)
- 275 – NIR(BP1): MaxMax XNiteBPB band pass filter (650nm to 787nm; 5% low cut – 5% high  
276 cut)

277 5-Band image composites were created by overlaying and rectifying the different wavelength  
278 bands based on manually located ground control points in each image. Parts of the scenes not covered  
279 by all image bands were cropped before further analysis. No suitable photos were collected with the  
280 NIR(BP1) filter from the Helikite platform, so this band is missing from the 'from helikite' image  
281 stack.  
282

283 *Image segmentation and object analysis*

284 To obtain image objects and enable calculation of meaningful feature values from these, all  
285 images were segmented in Trimble eCognition image analysis software (Trimble, 2010) at two levels.  
286 A first segmentation level was created using the Red and NIR(R72) bands only, which was suitable  
287 for delineation of vegetated areas. At a scale parameter of 200 groups of objects best followed the  
288 outlines of the main vegetation patches, while individual objects fully delineated the majority of  
289 smaller patches ( $\pm$  25cm diameter). 'Shape' and 'compactness' parameters were chosen as 0.5 and  
290 0.1, since at this level object delineation should be determined by both shape and spectral  
291 characteristics of the data, while the shape of the objects should be able to take on any form (i.e. low  
292 compactness). Next the image objects at this first level were sub-segmented at a second level to obtain  
293 objects that delineated the more detailed structure of the plants. The same image bands were used at  
294 this level, but a scale parameter of 20 and shape and compactness parameters of 0.9 and 0 were  
295 chosen. The latter two parameters indicate that object delineation was mostly determined by its shape  
296 and could take on any form. For all images these segmentation settings resulted in the creation of  
297 rather elongated sub-objects, clearly representing the 'hair-like' shape of some of the macrophytes  
298 (see image close up in Figure 2).

299 A large number of features are available in eCognition to describe the shape and texture of  
300 image objects and many more can be 'designed' by the user. Due to their large number, selection of  
301 the most suitable features to classify species can involve similar procedures as used for spectral band  
302 selection. However the user can also use expert opinion to select the most meaningful features based  
303 on visual interpretation of the image data. A combined approach was applied for this study. The  
304 following two features were developed based on expert opinion and thought to describe the structural  
305 difference between macrophyte species:

306  
307 1) Mean length/width ratio of sub-objects.

308 This feature value is obtained by calculating the length/width ratio for all level two objects  
309 and averaging these within each first level object. The value seems to quantify the presence of a 'hair-  
310 like' structure in particularly Water Crowfoot patches.

311  
312 2) Mean standard deviation red of sub-objects.

313 This feature value is obtained by calculating the standard deviation of pixel values for all level two  
314 objects and averaging these within each first level object. The value seems to represent a relatively  
315 strong spectral difference between the stems and leaves of the Water Crowfoot plants.

316  
317 A further selection of features for this analysis was taken from a range of texture measures  
318 that are standard included in the eCognition software. The eCognition 'Feature Selection Tool' used  
319 for this purpose determines the most suitable features from a given selection. This resulted in a  
320 selection of three Grey Level Co-occurrence Matrix features (GLCM), which are texture measures as  
321 described by Haralick et al. (1973). The measures quantify the amount of variability between adjacent  
322 pixels that make up an object. In this case the measures for contrast, dissimilarity and homogeneity  
323 were tested. The various types of texture features and their different calculation methods tend to  
324 produce strongly correlated values and are likely to result in similar difference estimates.

325  
326 For the objects representing each of the species the following range of feature values were  
327 calculated and exported into SPSS for further difference analysis:

- 328  
329 – Mean Length/ Width Sub-objects  
330 – Mean standard deviation red of sub-objects  
331 – GLCM Contrast (quick 8/11 all dir.)  
332 – GLCM dissimilarity (quick 8/11 all dir.)  
333 – GLCM homogeneity (quick 8/11 all dir.)

334  
335 In addition to this the average reflectance values for the objects in each band were calculated,  
336 exported and compared in the same manner. Because the number of Pondweed objects for some  
337 images were relatively small, a non-parametric Mann-Whitney U test was executed to determine to  
338 what extent there was a significant difference between object feature values of each macrophyte  
339 species.

340

## 341 **Results**

### 342 *Spectral species discrimination*

343 Table 1 shows a summary of the sample numbers and depth ranges measured for each of the  
344 macrophyte species. Each sample has a spectral range of 350 - 1050nm and a sampling interval of  
345 1.5nm. An example spectrum is shown in Figure 3, which also shows the attenuation coefficient of  
346 water ( $K_d$ ). Suspended load is mostly absent from the sampled streams, so no water quality  
347 adjustments were made.

348 The results of the ANOVA analysis for the submerged vegetation spectra and those of  
349 vegetation put onto the canvas are presented in Figures 4 and 5. The dark grey histograms indicate the

350 wavelength ranges where significant differences were found between combinations of two or more  
351 different macrophyte species with a 99% confidence level. The light grey parts of the histograms  
352 indicate differences at 95% confidence level. The ANOVA test resulted in a slightly narrower range  
353 of suitable wavelengths for the submerged vegetation spectra compared to those estimated for  
354 vegetation taken out of the water. For submerged spectra differences at 95% significance level were  
355 only found for the 500 to 600nm and the 850 to 950nm wavelength regions (Figure 4). For 99%  
356 significance level this range was reduced to a region of visible green light between 525 and 576nm  
357 and a very narrow section of the IR between 913 and 926nm. The latter finding is quite remarkable as  
358 the IR wavelengths are expected to be strongly affected by water absorption. The range of significant  
359 spectra measured on the canvas is wider (Figure 5), but considerable areas with too much overlap  
360 between species remain. Similar to the submerged spectra significant differences are found in the VIS  
361 wavelengths between 500 and 600nm. However, the range of significant NIR bands is different.  
362 Significant wavelengths for spectra on canvas start at the beginning of the red edge (from 691nm) and  
363 become less pronounced from 823nm onwards. The secondary y-axis in both figures indicates the  
364 number of significant species combinations for each grey wavelength region. For both sets of spectra  
365 only significant differences were found between Milfoil and Pondweed or Milfoil and Crowfoot.  
366 Differences between Pondweed and Crowfoot were not significant at 95% for any of the wavelengths  
367 both above and below the water surface.

368 Table 2 shows the combined results of the CART and J-M analysis for the submerged  
369 vegetation spectra. The table lists the J-M distance values from band selection resulting from CART  
370 as well as the best performing combinations of 2 to 6 bands, which were randomly drawn from the  
371 significant ANOVA range and the full data set. Results of CART analysis performed on Pondweed  
372 and Crowfoot data only are also included. Best performing band combinations are highlighted. Table  
373 3 shows the same information for the vegetation spectra measured on canvas. The J-M distance  
374 analysis results show that despite the significant difference between species for individual  
375 wavelengths in the ANOVA analysis, actual separability of the species is not necessarily possible.  
376 Complete separability of Water Milfoil and either of the other two species is possible when the  
377 spectra are measured without the influences of water. However, J-M values only get up to 1.44 for  
378 separability between Water Crowfoot and Pondweed. The J-M values become lower when the  
379 vegetation is covered by a variable water layer. Better results are achieved when the number of bands  
380 used in the analysis increases, however, attempts using up to 6 bands did still not result in the  
381 recommended minimum J-M distance of 1.9. For 6 bands highest values of 1.87 were obtained for  
382 Pondweed and Water Milfoil, both other combinations had lower values: 1.66 for Crowfoot and  
383 Milfoil and 1.62 for Pondweed and Crowfoot. The latter value was obtained for a combination with  
384 one band less.

385

### 386 *OBIA species discrimination*

387 Figures 6A-D show the outlines of the first segmentation level of objects in each image taken  
388 from the four different platforms. Objects representing Pondweed and Water Crowfoot were manually  
389 selected and are outlined in white and grey respectively. Table 4 shows the total number of objects for  
390 each of the two species available for analysis. Table 5 shows the significance levels of the Mann-  
391 Whitney U test for difference in object feature values between both macrophyte species, as observed  
392 from each platform. More detailed information about the distribution of each sample is shown in the  
393 boxplots of Figures 7A-F. The data indicates that the best results for separating the macrophytes were  
394 achieved with the highest resolution data. Objects from the image taken from a tripod just above the  
395 water surface show significant differences for all object shape and texture features tested. The lowest  
396 p values were obtained for the difference test using some of the spectral band values only (i.e. red,  
397 BP1 and R72+BP1). All lower resolution data show fewer significantly different object features. The  
398 feature that performs best is the 'mean length/width ratio of the sub-objects'. The remaining texture  
399 features all perform similarly. Figures 7 A-H show boxplots that illustrate the distribution of values  
400 for a selection of 8 features (red, green, blue, BP1, R72, mean length/width ratio sub-objects, mean  
401 standard deviation sub-objects and GLCM contrast).



402

## 403 **Discussion and implications**

### 404 *Spectral species discrimination*

405 The results showed that water depth will be a limiting factor for the classification of species  
406 from remote sensing images. Spiked Water Milfoil was indicated as spectrally distinct from the other  
407 species across the observed range of water depths with ANOVA analysis, but this was not confirmed  
408 by Jeffries-Matusita distance analysis. In particular Water Crowfoot and Pondweed could not be  
409 discriminated at 95% significance level. J-M distance analysis values confirmed these observations.  
410 The latter two species are spectrally so similar that they could not be discriminated without the effect  
411 of an overlying water column either.

412 Both submerged macrophytes and those taken out of the water on the canvas show significant  
413 differences in the VIS wavelength range between 500 and 600nm. This range corresponds with useful  
414 bands found by O'Neill et al. (2011) who found that most marked differences between benthic classes  
415 occurred in the green spectral range between 500 and 600 nm, which coincides with lower  $K_d$  values.  
416 It also coincides with the photosynthetic pigment absorption minimum between that lies between 555  
417 and 565. The position of the significant NIR range is rather different for each of the two data sets. The  
418 range including the red-edge, found for the spectra on canvas, corresponds with findings for most  
419 terrestrial vegetation species, which show most variation around this region. The same NIR region  
420 does not result in significant differences for the submerged spectra, which was expected considering  
421 the high variability in this wavelength region due to the increased  $K_d$ . Remarkably however, a small  
422 region of wavelengths between 850 and 950nm is selected in the ANOVA analysis and some of the  
423 NIR wavelengths contribute to the combinations that result in best separability. For emergent species  
424 Adam and Mutanga (2009) also identified several wavelengths in this part of the NIR as most useful  
425 for discrimination between vegetation species.

426 The results indicate that for accurate classification of any of the submerged macrophytes more  
427 than 6 wavelength bands will be required. Depth clearly has an influence here as for the spectra  
428 measured on canvas sufficient distance values were achieved for two out of the three species  
429 combinations with three bands or less. Comparisons with results from other studies are difficult due to  
430 differences in experimental set up, but Lee et al. (2011) managed to discriminate between most algal  
431 species with as little as two bands despite attenuation from the overlying water column. The suitable  
432 wavelengths found in their study related to variations in colour and presence of unhealthy cellular  
433 structures. They mostly fall outside the wavelength ranges found in this study, which is most likely  
434 due to the rather different vegetation types that they looked at. To discriminate between Eelgrass and  
435 associated bottom types in non-water corrected remote sensing images of much deeper marine  
436 conditions (1-30m) O'Neill et al. (2011) needed ten bands of 4 nm bandwidth. In their analysis they  
437 include spectral derivatives ( $R'$ ) and band ratios. Using the same data corrected for water depth they  
438 only needed 3 bands, though a classification based on these bands turned out to be less accurate. Their  
439 findings included bands covering the peak ( $R'566$ ) and shoulders (500-530 &  $R'580$ ) of the green  
440 reflectance maxima. This corresponds with the findings of this study, which identified significant  
441 ANOVA results in the green wavelength region and bands from this region were included in the  
442 selections with the highest J-M distance values. Their data did not include wavelengths beyond  
443 800nm, which have proven most effective in this study.

444 CART analysis applied to the spectra on canvas consistently selected the 711nm band to  
445 separate between the 'green' and the 'red' (milfoil) macrophytes, followed by bands of blue light (460  
446 - 480nm) to further separate between the two 'green' species. The latter bands fall outside the range  
447 selected as significant with the ANOVA test. CART analysis applied to the significant wavelengths of  
448 submerged species produces better J-M values than CART applied to all wavelengths. The bands  
449 selected in the latter case are also mostly from the green light region and IR wavelengths beyond  
450 950nm. The highest J-M distance values were not achieved for band combinations selected through  
451 CART and also not always for band combinations taken from the statistically significant regions.  
452 Although distances were not calculated for all band combinations, this suggests that the combined

453 ANOVA and CART band selection method may not be suitable as a data dimensionality reduction  
454 method in this situation. To confirm this analysis should be repeated with other band selection  
455 methods.  
456

#### 457 *OBIA species discrimination*

458 The first part of the analysis showed how the macrophyte species Pondweed and Water  
459 Crowfoot are spectrally so similar that even without water column influences they are difficult to  
460 distinguish. These results indicate that information other than spectral reflectance needs to be  
461 incorporated in image analysis to enable accurate classification of these species. The subsequent  
462 testing of difference between species based on a number of texture and shape features confirms the  
463 potential to do so. The good performance of the 'length/width ratio of sub-objects' feature confirms  
464 that our initial visual interpretation of the image data was good and that such expert knowledge can be  
465 useful for species discrimination. The feature does however not perform very well for the images  
466 taken from the highest platform. This could indicate that the possibility to use the length/width shape  
467 feature to discriminate the species deteriorates at a less detailed scale. Sufficient resolution may be  
468 needed to produce the more elongated object shapes for Water Crowfoot during segmentation.

469 In general contrast features performed well, which confirmed visual interpretation of the  
470 images showing clear variation in spectral contrast amongst the two species. The spectral features  
471 perform worst with some not allowing discrimination of the species at any scale (e.g. red band). This  
472 result corresponds to some extent with the ANOVA test results which showed only narrow regions of  
473 wavelengths with sufficient difference between the macrophyte species. The best performing bands  
474 however do not seem to correspond exactly with the significant wavelength regions (e.g. blue band).  
475 The poor performance of the spectral features in general does support the original expectation that  
476 incorporation of shape and texture information is essential for successful classification of SAV. It is  
477 however unclear why there is considerable variation in separability amongst the different image scales  
478 as the spectral features are not expected to be scale dependent.

479 In general images produced with the Helikite were of reasonable quality, but only the images  
480 taken from the tripod and the bridge were consistently of good quality. In particular collection of NIR  
481 photos from the more elevated platforms was difficult due to limited availability of the camera  
482 autofocus in combination with the light blocking filters. The NIR(R72) band of the image taken from  
483 the pole was especially blurry, which may have affected some of the results. Texture features are  
484 likely to be more dependent on image focus than shape features like the l/w ratio, but further  
485 investigations of such effects is required. No pre-processing was applied to any of the data. Some  
486 preprocessing could have further improved data quality, as sunglint caused locally high reflectance  
487 values in most image bands. The high values will have affected contrast calculations, resulting in an  
488 overestimation of object contrast. Its quantitative effect on the presented results is currently not  
489 known.

490 The first attempt to use an UAS to collect remote sensing data for submerged macrophyte  
491 monitoring was not overly successful. This was to a large extent due to the type of UAS and multi-  
492 spectral sensor used. Due to a combination of camera weight, wind conditions, presence of  
493 surrounding vegetation, people and telegraph lines it was impossible to achieve elevations higher than  
494 the telescopic pole with the Helikite and therefore scale wise this platform did not contribute extra  
495 information to this study and the range of scales studied was limited. Because the exact location of the  
496 camera from this platform was most difficult to control, only a very small section of the images was  
497 ultimately suitable for analysis. It also made manual image correction rather challenging. The Helikite  
498 required restricted environmental conditions, especially when paired with a relatively heavy camera.

499 Similar to the spectral discrimination analysis, the object-based features may 'interact' and  
500 perform better when a number of different features are combined to discriminate between plant  
501 species. This has currently not been attempted yet. So far the difference tests are statistical exercise  
502 only. Better results are also likely with the inclusion of band ratios. To find out to what extent the  
503 features really enable accurate classification of the macrophyte species will need further testing on  
504 more extensive image data, covering larger areas and a wider range of situations.

505 *Implications*

506 The foregoing discussion suggests that it is not possible to accurately map submerged aquatic  
507 vegetation in the chalk streams, using spectral information only, even if water depth correction of the  
508 vegetation spectra is possible. However, despite strongly increasing  $K_d$  the NIR wavelengths still  
509 show considerable amounts of reflectance at the submergence depths observed for the chalks stream  
510 macrophyte species. The observation that wavelengths between 920 and 950nm showed potential to  
511 discriminate between at least two of the submerged species, was remarkable and use of this  
512 wavelength region should be further explored. Although spectral separability in the NIR wavelengths  
513 was not clearly confirmed by J-M distance analysis, the information in any case enhances shape and  
514 textural variation in the data, which benefits the OBIA approach. The inclusion of texture and shape  
515 features in image analysis through OBIA clearly shows promise for the mapping of SAV from image  
516 data. Further work is however also required on scale dependency, as shape and texture features did  
517 not show significant differences between the species for all scale levels.

518 Finally, to make the presented techniques interesting for river managers for mapping and  
519 monitoring of SAV patterns in small streams the proposed approach will need to be converted into a  
520 tool that can produce consistent results for a wide range of fluvial situations with the smallest amount  
521 of input from operators. The OBIA approach has already shown to be a useful approach in other  
522 settings, by eliminating the need for an image data sample for classification after a rule set has been  
523 created (e.g. Walker and Blaschke, 2008). Based on the results of this study it is not inconceivable  
524 that a similar tool can be developed for the benefit of shallow clear stream environments.  
525

526 **Acknowledgments**

527 The fieldwork for this project was funded by the University of Worcester and the Earth and  
528 Space Foundation. The field spectroradiometer was obtained on loan from the NERC Field  
529 Spectrometry Facility (FSF) (loan ref 569.1208 and 550.1207). Furthermore we would like to thank  
530 Langford Trust Nature Reserve for access to the River Wylye field site and Justin Kirby for his help  
531 with the fieldwork.  
532

533 **References**

- 534  
535 Adam, E., Mutanga, O., 2009. Spectral discrimination of papyrus vegetation (*Cyperus papyrus* L.) in  
536 swamp wetlands using field spectrometry. *ISPRS Journal of Photogrammetry and Remote*  
537 *Sensing*, 64, 612-620.
- 538 Blaschke, T., Johansen, K., Tiede, D., 2011. Object based image analysis for Vegetation mapping and  
539 Monitoring. In: Weng, Q. (Ed.): *Advances in Environmental Remote Sensing: Sensors,*  
540 *Algorithms, and Applications*. Taylor & Francis, London, 241-271.
- 541 Breiman, L., Friedman, J.H., Olshen, R.A., Stone, C.J., 1984. *Classification and Regression Trees*.  
542 Chapman & Hall (Wadsworth, Inc.), New York.
- 543 Dekker, A.G., Phinn, S.R., Anstee, J., Bissett P., Brando, V.E., Casey, B., Fearn, P., Hedley, J.,  
544 Klonowski, W., Lee, Z.P., Lynch, M., Lyons, M., Mobley, C., Roelfsema, C., 2011.  
545 Intercomparison of shallow water bathymetry, hydro-optics, and benthos mapping techniques in  
546 Australian and Caribbean coastal environments. *Limnology and Oceanography-Methods*, 9,  
547 396-425. DOI: 10.4319/lom.2011.9.396
- 548 ENVI, 2004. *ENVI User's Guide, ENVI Version 4.1*. Research Systems Inc.
- 549 Flynn, N.J., Snook, D.L., Wade, A.J., Jarvie, H.P., 2002. Macrophyte and periphyton dynamics in  
550 a UK Cretaceous chalk stream: the River Kenneth a tributary of the Thames. *The Science*  
551 *of the Total Environment*, 282-283, 143-257.
- 552 Giardino, C., Candiani, G., Bresciani, M., Lee, Z., Gagliano, S., Pepe, M., 2012. BOMBER: A tool  
553 for estimating water quality and bottom properties from remote sensing images. *Computers &*  
554 *Geosciences*, 45, 313–318. DOI: 10.1016/j.cageo.2011.11.022

- 555 Gilvear, D., Hunter, P., Higgins, T., 2007. An experimental approach to the measurement of the  
556 effects of water depth and substrate on optical and near infra-red reflectance: a field-based  
557 assessment of the feasibility of mapping submerged instream habitat. *International Journal of*  
558 *Remote Sensing*. 28 (10), 2241-2256.
- 559 Haralick, R.M., Shanmugam, K., Dinstein, I., 1973. Textural Features for Image Classification  
560 Systems. *IEEE Transactions on Man and Cybernetics*. 3 (6), 610 – 621.
- 561 Hedley, J.D., Roelfsema, C.M., Phinn, S.R., Mumby, P.J., 2012. Environmental and Sensor  
562 Limitations in Optical Remote Sensing of Coral Reefs: Implications for Monitoring and  
563 Sensor Design. *Remote Sensing*, 4, 271-302. DOI: 10.3390/rs4010271
- 564 Hill, R.A., O'Hare, M.T., Stillman, R.A., Gozlan, R.E., 2009. Hyperspectral remote sensing of river  
565 macrophyte vegetation: towards an assessment of wildfowl and fish habitat quality. In:  
566 *Proceedings of the RSPSoc Annual Conference: New Dimensions in Earth Observation*, 8-11  
567 September 2009, Leicester.
- 568 Karpouzli, E., Malthus, T.J., Place, C.J., 2004. Hyperspectral discrimination of coral reef benthic  
569 communities in the western Caribbean. *Coral Reefs*. 23, 141-151. DOI: 10.1007/s00338-003-  
570 0363-9
- 571 Laliberté, A.S., Rango, A., 2009. Texture and scale in object-based analysis of subdecimeter  
572 resolution UAV imagery. *IEEE Transactions on Geoscience and Remote Sensing*. 47(3), 761-  
573 770.
- 574 Lee, B.S., McGwire, K.C., Fritsen, C.H., 2011. Identification and quantification of aquatic vegetation  
575 with hyperspectral remote sensing in western Nevada rivers, USA. *International Journal of*  
576 *Remote Sensing*. 32, 9093-9117.
- 577 Legleiter, C.J., Roberts, D.A., 2009. A forward image model for passive optical remote sensing of  
578 river bathymetry. *Remote Sensing of Environment*. 113, 1025-1045. DOI:  
579 10.1016/j.rse.2009.01.018
- 580 Marcus, W.A., Fonstad, M.A., 2008. Optical remote mapping of rivers at sub-meter resolutions and  
581 watershed extents. *Earth Surface Processes and Landforms*, 33, 4-24. DOI: 10.1002/esp.1637
- 582 Maritorena, S., Morel, A., Gentili, B., 1994. Diffuse-reflectance of oceanic shallow waters - influence  
583 of water depth and bottom albedo. *Limnology and Oceanography*. 39, 1689-1703.
- 584 O'Hare, M.T., McGahey, C., Bissett, N., Cailes, C., Henville, P., Scarlett, P., 2010. Variability in  
585 roughness measurements for vegetated rivers near base flow, in England and Scotland. *Journal*  
586 *of Hydrology*. 385, 361-370. DOI: 10.1016/j.jhydrol.2010.02.036
- 587 O'Neill, J.D., Costa, M., Sharma, T., 2011. Remote sensing of shallow coastal benthic substrates: In  
588 situ spectra and mapping of Eelgrass (*Zostera marina*) in the Gulf Islands National Park  
589 Reserve of Canada. *Remote Sensing*. 3, 975-1005. DOI: 10.3390/rs3050975
- 590 Phinn, S.R., Roelfsema, C.M., Mumby, P.J., 2012. Multi-scale, object-based image analysis for  
591 mapping geomorphic and ecological zones on coral reefs. *International Journal of Remote*  
592 *Sensing*. 33, 3768-3797. DOI: 10.1080/01431161.2011.633122
- 593 Trimble, 2010. eCognition® Developer 8.64.0 user guide, Trimble: Munich, Germany.
- 594 Van der Werff, H.M.A., Van der Meer, F.D., 2008. Shape-based classification of spectrally identical  
595 objects. *ISPRS Journal of Photogrammetry and Remote Sensing*. 63 (2), 251-258.
- 596 Urbanski, J.A., Mazur, A., Janas, U., 2009. Object-oriented classification of QuickBird data for  
597 mapping seagrass spatial structure. *Oceanological and Hydrobiological Studies*. 38, 27-43.  
598 DOI: 10.2478/v10009-009-0013-9
- 599 Vahtmäe, E., Kutser, T., Martin, G., Kotta, J., 2006. Feasibility of hyperspectral remote sensing for  
600 mapping benthic macroalgal cover in turbid coastal waters - a Baltic Sea case study. *Remote*  
601 *Sensing of Environment*. 101, 342-351. DOI: 10.1016/j.rse.2006.01.009
- 602 Visser, F., Hill, R.A., 2011. Application of hyperspectral image data for species detection and  
603 biomass estimation of submerged macrophytes in UK chalk streams. In: *Proceedings of the*  
604 *EARSeL 7th SIG-Imaging Spectroscopy Workshop*, Edinburgh, UK, 11-13 April 2011.
- 605 Visser, F., Wallis, C., 2010. Object-based analysis and multispectral low-altitude remote sensing for  
606 low-cost mapping of chalk stream macrophytes. *The International Archives of the*  
607 *Photogrammetry, Remote Sensing and Spatial Information Sciences*. XXXVIII-4/C7.

- 608 Walker, J. S., Blaschke, T., 2008. Object-based land-cover classification for the Phoenix metropolitan  
609 area: optimization vs. transportability. *International Journal of Remote Sensing*. 29 (7), 2021-  
610 2040.
- 611 Wang, C., Philpot, W.D., 2007. Using airborne bathymetric lidar to detect bottom type variation in  
612 shallow waters. *Remote Sensing of Environment*. 106, 123-135. DOI:  
613 10.1016/j.rse.2006.08.003
- 614 Yang, Y., Xiao, Y., Segal, M., 2005. Identifying differentially expressed genes from microarray  
615 experiments via statistic synthesis. *Bioinformatics*. 21, 1084-1093. DOI:  
616 10.1093/bioinformatics/bti108
- 617

618 **Figure captions**

619

620 Figure 1: The transmission spectra of BP1 bandpass and CC1 and R72 blocking filters based on  
621 manufacturers specifications (maxmax.com). Submerged macrophyte spectrum included with dashed  
622 line for illustration.

623

624 Figure 2: Close-up of sub-objects in ‘from tripod’ image. Left: Pondweed objects. Right: more  
625 elongated Water Crowfoot objects.

626

627 Figure 3: Attenuation of reflectance from Water Crowfoot for submergence depths between 1.5 and  
628 40cm (example based on data collected during this study).

629

630 Figure 4: Frequency of statistically significant differences between three submerged macrophyte  
631 species with ANOVA analysis. Bars show number of significantly different combinations obtained  
632 (dark grey 99%; light grey 95%). Spectra represent min, max and average signatures for each of the  
633 species.

634

635 Figure 5: Frequency of statistically significant differences for three out-of-the-water macrophyte  
636 species with ANOVA analysis. Bars show number of significantly different combinations (dark grey  
637 99% significant; light grey 95% significant).

638

639 Figures 6 A-D: A selection of image ‘bands’ with segmentation object outlines: A) from tripod  
640 NIR(R72) band; B) from bridge Green band; C) from pole NIR(BP1) band; D) from helikite  
641 NIR(R72) band. In all images white object outlines represent Pondweed, grey Water Crowfoot and  
642 black Unclassified.

643

644 Figure 7: Boxplots illustrating the object feature values for 8 features (A-H), comparing Pondweed  
645 and Water Crowfoot objects as derived from images taken from four different platforms.

646

647

648

649 ***TABLES***

650

651 Table 1: Type and number of submerged vegetation spectral samples

Macrophyte species	N	Depth range (cm)
Pondweed	60	10-25
Water Crowfoot	37	2-40
Water Milfoil	66	3-50

652

653

654 Table 2: Results of the Jeffries-Matusita distance analysis for combinations of submerged Pondweed,  
 655 Water Crowfoot and Spiked Water Milfoil. White font indicates highest achieved distance value for  
 656 discriminating a pair of species; intermediate grey shade indicates highest distance value for given  
 657 band combination; light grey second best.  
 658

No. Bands	Band selection method	Wavelengths (nm)	J-M distance value for species combination		
			Pondweed - Milfoil	Crowfoot - Milfoil	Pondweed - Crowfoot
2	Random from significant wavelengths	555; 935	<b>1.08</b>	<b>0.61</b>	<b>0.40</b>
	Random from all wavelengths	1054; 426	0.54	0.10	0.30
		609; 816	0.67	0.45	0.09
3	Random from significant wavelengths	935; 544; 555	1.40	0.82	<b>0.75</b>
	Random from all wavelengths	848; 539; 489	<b>1.45</b>	<b>1.21</b>	0.34
		912; 756; 884	1.08	0.61	0.48
4	CART with all wavelengths	545; 576; 966; 555	1.54	1.31	0.66
	CART with all wavelengths; No Milfoil	533; 689; 997; 550	1.61	1.18	0.85
	Random from significant wavelengths	577; 927; 919; 568	1.69	<b>1.37</b>	0.88
		553; 923; 914; 525	<b>1.72</b>	1.15	<b>1.14</b>
	Random from all wavelengths	868; 522; 892; 1011	0.97	0.58	0.42
		830; 639; 813; 773	1.08	0.96	0.28
5	CART with significant wavelengths	543; 926; 555; 537; 923	1.72	1.20	1.26
	Random from significant wavelengths	535; 925; 914; 554; 540	1.78	1.40	1.25
		562; 925; 540; 891; 573	1.72	1.49	0.87
	Random from all wavelengths	935; 559; 939; 544; 555	1.77	<b>1.51</b>	1.10
		469; 911; 562; 514; 703	<b>1.81</b>	1.33	<b>1.62</b>
6	CART with significant wavelengths; No Milfoil	533; 525; 923; 553; 913; 917	1.80	1.53	1.27
	Random from significant wavelengths	535; 919; 548; 575; 924; 561	<b>1.87</b>	1.60	<b>1.45</b>
	Random from all wavelengths	920; 566; 925; 914; 554; 540	1.84	<b>1.66</b>	1.40

659

660



661 Table 3: Results of the Jeffries-Matusita distance analysis for combinations of Pondweed, Water  
 662 Crowfoot and Spiked Water Milfoil measured on canvas sheet. White font indicates highest achieved  
 663 distance value for discriminating a pair of species; intermediate grey shade indicates highest distance  
 664 value for given band combination; light grey second best.

No. Bands	Band selection method	Wavelengths (nm)	J-M distance value for species combination		
			Pondweed - Milfoil	Crowfoot - Milfoil	Pondweed - Crowfoot
3	CART with all wavelengths	711; 465; 483	1.84	1.69	0.73
	CART with all wavelengths; No Milfoil	465; 535; 483	<b>2.00</b>	1.93	0.77
4	Random from all wavelengths	545; 576; 966; 555	2.00	<b>1.99</b>	1.18
	Random from significant wavelengths	710; 752; 522; 834	2.00	1.98	1.26
5	Random from all wavelengths	543; 926; 555; 537; 923	2.00	1.98	<b>1.44</b>

665  
666

667 Table 4. Object sample numbers N for each macrophyte and location.  
668

	N Pond- weed	N Water Crowfoot
From tripod	12	21
From bridge	2	14
From helikite	3	8
From pole	6	9

669  
670

671 Table 5. Results for the Mann-Whitney U non-parametric test of similarity. Shaded results are  
 672 significant at 95%.  
 673

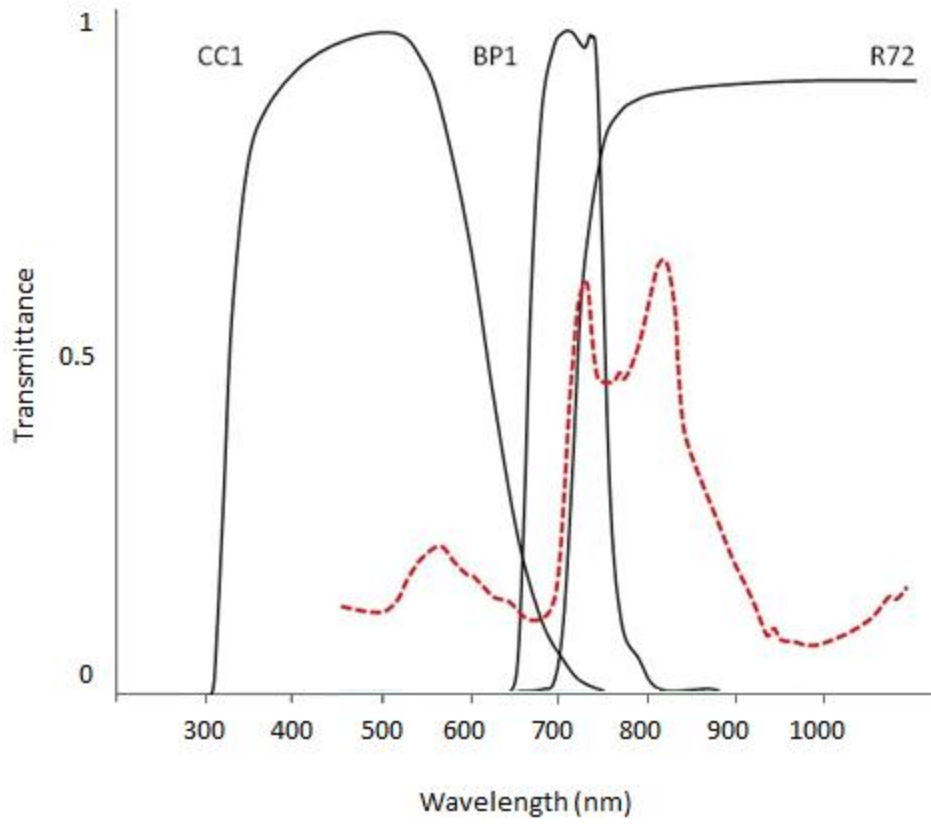
Location	Test statistic	Mean R	Mean G	Mean B	Mean BP1	Mean R72	Mean R72+BP1
	Significance						
from tripod (1.5m)	U	108	57	68	131	113	121
	P	0.50	0.00	0.02	0.68	0.41	0.75
from bridge (3m)	U	7	7	9	6	8	5
	P	0.33	0.33	0.50	0.27	0.42	0.20
from helikite (~5m)	U	3	7	9		0	
	P	0.12	0.38	0.83		0.02	
from pole (5.4m)	U	20	16	9	15	10	16
	P	0.46	0.22	0.04	0.18	0.05	0.22

674  
675

Location	Test statistic	Mean Length/Width sub-objects	Mean Stdev Red Sub-objects	Stdev Red	GLCM Contrast (quick 8/11) (all dir.)	GLCM Dissimilarity (quick 8/11) (all dir.)	GLCM Homogeneity (quick 8/11) (all dir.)
	Significance						
from tripod (1.5m)	U	16	30	46	25	27	33
	P	0.00	0.00	0.00	0.01	0.00	0.00
from bridge (3m)	U	1	4	7	4	6	7
	P	0.03	0.15	0.33	0.15	0.27	0.33
from helikite (~5m)	U	0	2	7	2	2	2
	P	0.02	0.07	0.37	0.07	0.07	0.07
from pole (5.4m)	U	22	8	11	1	3	3
	P	0.61	0.03	0.07	0.00	0.00	0.00

676  
677

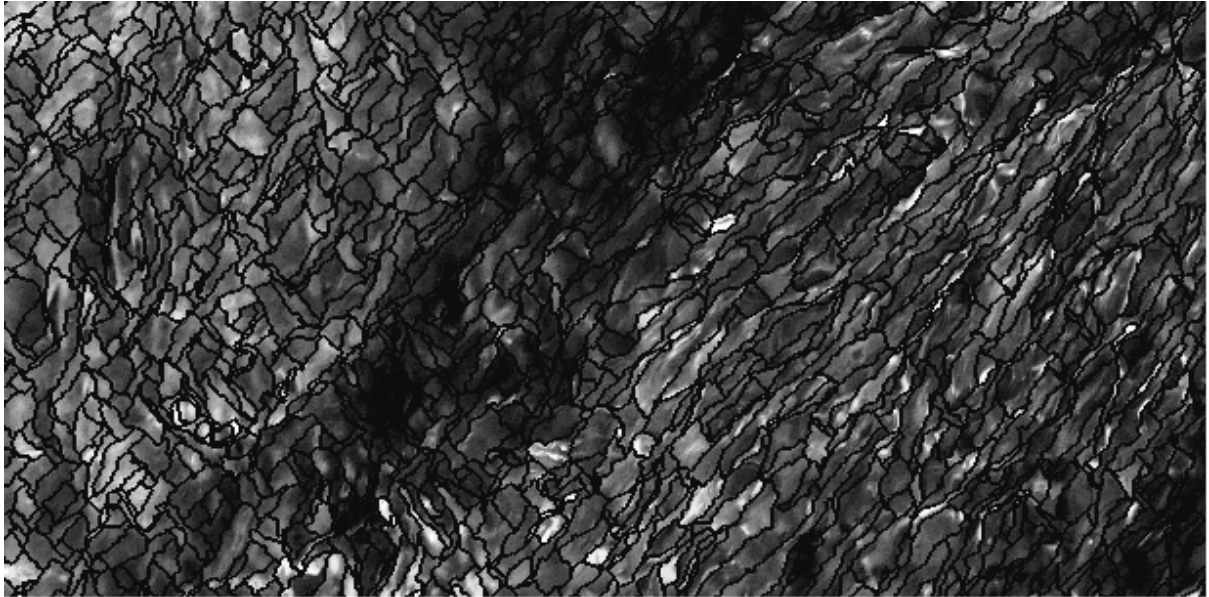
678 **Figures**



679

680 Figure 1

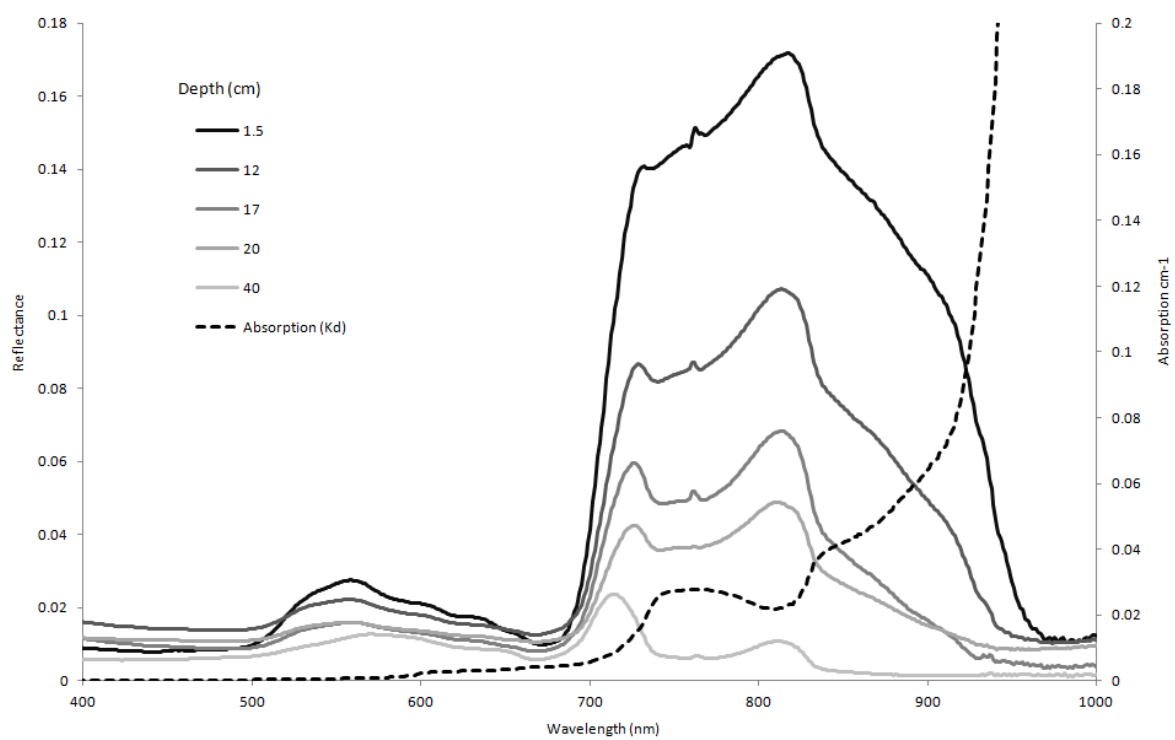
681



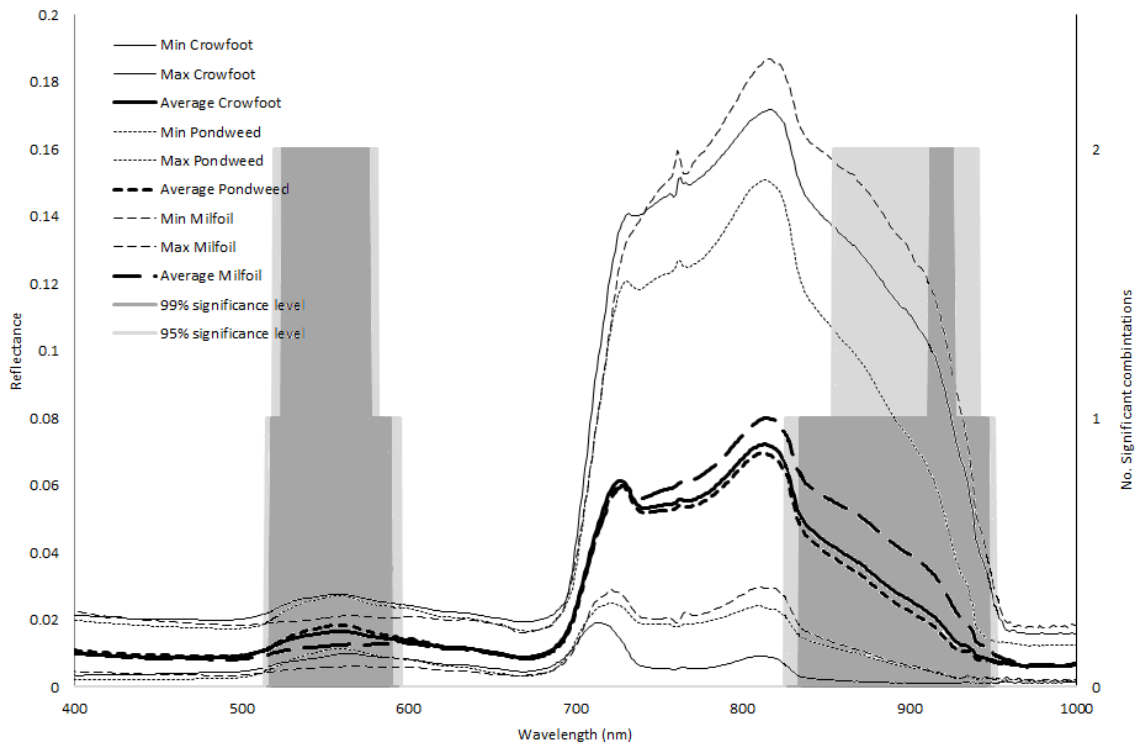
682

683 Figure 2

684



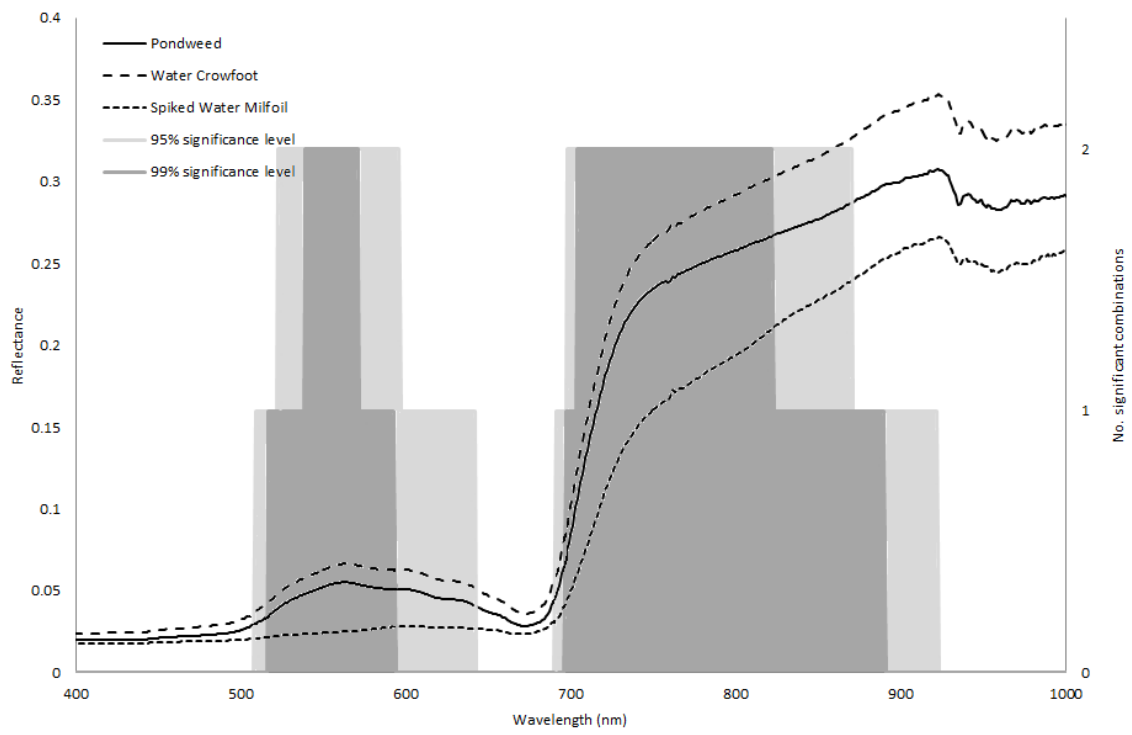
685  
686 Figure 3  
687



688

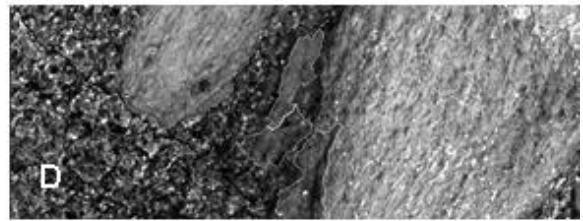
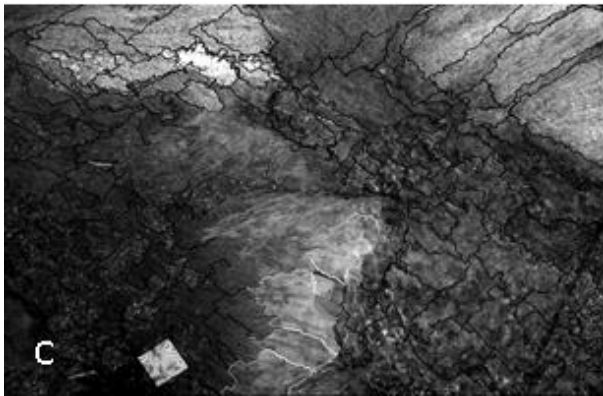
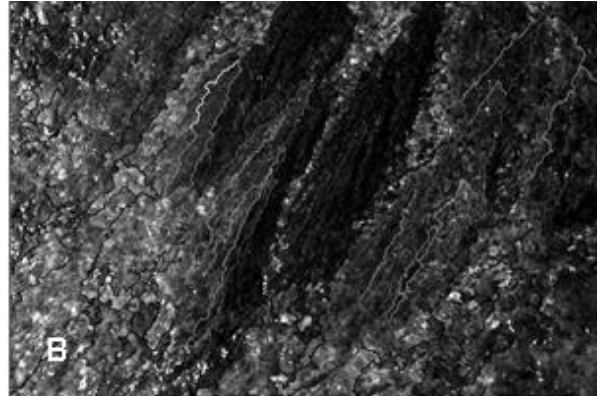
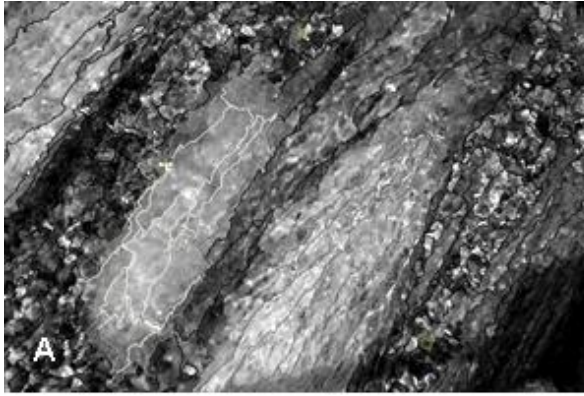
689 Figure 4

690



691 Figure 5  
 692  
 693

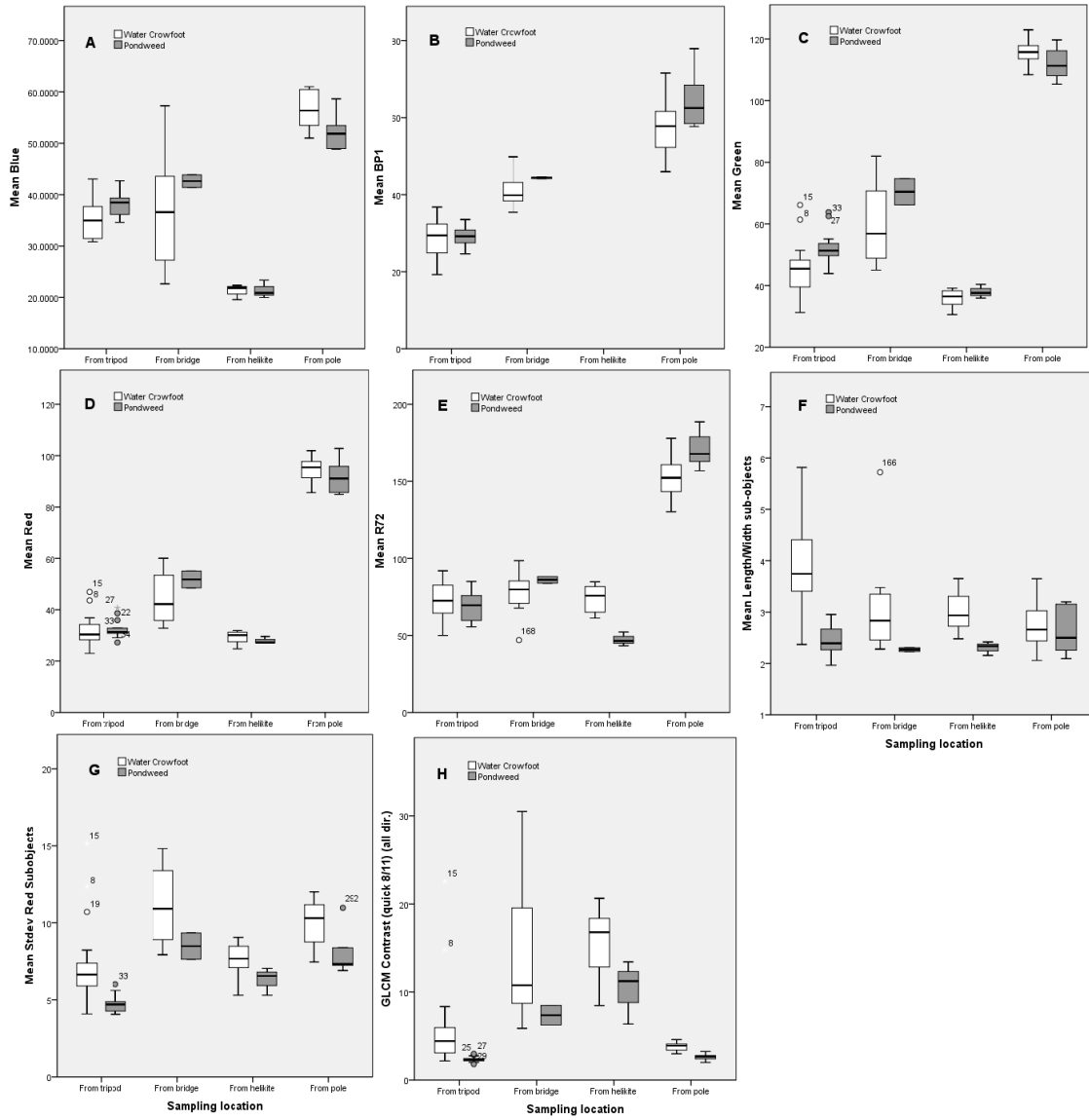




694

695 Figure 6

696



697

698 Figure 7